G3: Genes|Genomes|Genetics Early Online, published on November 4, 2016 as doi:10.1534/g3.116.033670

The first *Scube3* mutant mouse line with pleiotropic phenotypic alterations

Helmut Fuchs [a,b*], Sibylle Sabrautzki [a,c*], Gerhard KH Przemeck [a,b*], Stefanie Leuchtenberger [a], Bettina Lorenz-Depiereux [d], Lore Becker [a], Birgit Rathkolb [a,b,e], Marion Horsch [a], Lillian Garrett [a,f], Manuela A Östereicher [a], Wolfgang Hans [a], Koichiro Abe [g], Nobuho Sagawa [g], Jan Rozman [a,b], Ingrid L Vargas-Panesso [a,h,i], Michael Sandholzer [a], Thomas S Lisse [a,1], Thure Adler [a,j], Juan Antonio Aguilar-Pimentel [a], Julia Calzada-Wack [a,k], Nicole Ehrhard [a,l,2], Ralf Elvert [a,3], Christine Gau [a], Sabine M Hölter [a,f], Katja Micklich [a,e], Kristin Moreth [a], Cornelia Prehn [a], Oliver Puk [a,f,4], Ildiko Racz [m], Claudia Stoeger [a], Alexandra Vernaleken [a,h,i], Dian Michel [a,5], Susanne Diener [d], Thomas Wieland [d], Jerzy Adamski [a,b], Raffi Bekeredjian [n], Dirk H Busch [o], John Favor [d], Jochen Graw [f], Martin Klingenspor [p,q], Christoph Lengger [a], Holger Maier [a], Frauke Neff [a,k], Markus Ollert [r,s], Tobias Stoeger [t], Ali Önder Yildirim [t], Tim M Strom [d], Andreas Zimmer [m], Eckhard Wolf [e], Wolfgang Wurst [f,u,v,w], Thomas Klopstock [h,i,u,w], Johannes Beckers [a,b,x], Valerie Gailus-Durner [a,b], Martin Hrabě de Angelis [a,b,i,x]

[a] German Mouse Clinic, Institute of Experimental Genetics, Helmholtz Zentrum München, German Research Center for Environmental Health, Ingolstädter Landstr.1, 85764 Neuherberg, Germany

[b] Member of German Center for Diabetes Research (DZD), Ingolstädter Landstr.1, 85764 Neuherberg, Germany

[c] Research unit comparative medicine, Helmholtz Zentrum München, German Research Center for Environmental Health, Ingolstädter Landstr.1, 85764 Neuherberg, Germany

[d] Institute of Human Genetics, Helmholtz Zentrum München, German Research Center for Environmental Health, Ingolstädter Landstr.1, 85764 Neuherberg, Germany

[e] Chair for Molecular Animal Breeding and Biotechnology, Gene Center of the Ludwig-Maximilians-Universität München, Feodor-Lynen-Str. 25, 81377 München, Germany

[f] Institute of Developmental Genetics, Helmholtz Zentrum München, German Research Center for Environmental Health, Ingolstädter Landstr.1, 85764 Neuherberg, Germany

[g] Department of Life Science, Tokai University School of Medicine Shimokasuya 143, Isehara, Kanagawa 259-1193, Japan

[h] Department of Neurology, Friedrich-Baur-Institut, Ludwig-Maximilians-Universität München, Ziemssenstr. 1a, 80336 München, Germany

[i] German Center for Vertigo and Balance Disorders, Munich, Germany

[j] Institute of Stem Cell Research**,** Helmholtz Zentrum München, German Research Center for Environmental Health, Ingolstädter Landstraße 1, 85764 Neuherberg, Germany

[k] Institute of Pathology, Helmholtz Zentrum München, German Research Center for Environmental Health, Ingolstädter Landstr.1, 85764 Neuherberg, Germany

[l] Cedars-Sinai Medical Genetics Research Institute, 8700 Beverly Blvd., Davis Building, Los Angeles, CA 90048, USA

[m] Institute of Molecular Psychiatry, Medical Faculty, University of Bonn, Sigmund Freud Str. 25, 53127 Bonn, Germany

[n] Division of Cardiology, University of Heidelberg, Im Neuenheimer Feld 410, 69120 Heidelberg, Germany

[o] Institute for Medical Microbiology, Immunology and Hygiene, Technische Universität München, Trogerstrasse 9, 81675 Munich, Germany

[p] Chair of Molecular Nutritional Medicine, Technical University Munich, EKFZ – Else Kröner Fresenius Center for Nutritional Medicine, Gregor-Mendel-Str. 2, 85350 Freising-Weihenstephan, Germany

[q] ZIEL – Institute for Food and Health, Technical University Munich, Gregor-Mendel-Str. 2, 85350 Freising-Weihenstephan, Germany

[r] Department of Dermatology and Allergy, Biederstein, Klinikum rechts der Isar, Technische Universität München (TUM), Biedersteiner Str. 29, 80802 Munich, Germany

[s] Department of Infection and Immunity, Luxembourg Institute of Health, Esch-sur-Alzette, Luxembourg, and Department of Dermatology and Allergy Center, Odense Research Center for Anaphylaxis, University of Southern Denmark, Odense, Denmark

[t] Institute of Lung Biology and Diseases, Helmholtz Zentrum München, German Research Center for Environmental Health, Ingolstädter Landstr.1, 85764 Neuherberg, Germany

[u] DZNE - German Center for Neurodegenerative Diseases,Schillerstrasse 44, 80336 Munich, Germany

[v] Lehrstuhl für Entwicklungsgenetik, Technical University München-Weihenstephan, c/o Helmholtz Zentrum München, Ingolstädter Landstr. 1, 85764 Neuherberg, Germany

[w] Munich Cluster for Systems Neurology (SyNergy), Adolf-Butenandt-Institut, Ludwig-Maximilians-Universität München, Schillerstrasse 44, 80336 Munich, Germany

[x] Lehrstuhl für Experimentelle Genetik, Technische Universität München, 85350 Freising-Weihenstephan, Germany

[1] Present address: The Jackson Laboratory, Bar Harbor, Maine, USA

[2] Present address: Basic Medical Sciences, Osteopathic Medicine of the Pacific, Western University of Health Sciences, 309 E. Second Street, Pomona, CA, 91766, USA

[3] Present address: Sanofi-Aventis Deutschland GmbH, General Metabolism and Obesity, 65926 Frankfurt am Main, Germany

[4] Present address: ceGAT, Paul-Ehrlich-Straße 23, 72076 Tübingen, Germany

[5] Present address: Deutsches Zentrum für Luft- und Raumfahrt e.V., DLR Projektträger, Heinrich-Konen-Str. 1, 53227 Bonn, Germany

* First authors' equal contribution to the manuscript

Running title: Scube3 mutant mouse phenotype

Keywords:
SCUBE3
Systemic phenotype
Pleitropy
Paget disease of bone (PDB)
Mouse model

Corresponding author:
Prof. Dr. Martin Hrabě de Angelis, Helmholtz Zentrum München, German Research Center for Environmental Health (GmbH), Institute of Experimental Genetics, Ingolstädter Landstr.1, 85764 Neuherberg, Germany. Phone: +49 (0) 89-3187-3502. Fax: +49 (0) 89-3187-3500. E-mail address: hrabe@helmholtz-muenchen.de

ABSTRACT

The vertebrate *Scube* (Signal peptide, CUB and EGF-like domain-containing protein) family consists of three independent members *Scube1-3*, which encode secreted cell surface-associated membrane glycoproteins. Limited information about the general function of this gene family is available, and their roles during adulthood. Here, we present the first *Scube3* mutant mouse line *(Scube3*$^{N294K/N294K}$) that clearly shows phenotypic alterations by carrying a missense mutation in exon 8, and thus contributes to understand *SCUBE3* functions. We performed a detailed phenotypic characterization in the German Mouse Clinic (GMC). *Scube3*$^{N294K/N294K}$ mutants showed morphological abnormalities of the skeleton, alterations of parameters relevant for bone metabolism, changes in renal function and hearing impairments. These findings correlate with characteristics of the rare metabolic bone disorder Paget disease of bone (PDB), associated with the chromosomal region of human *SCUBE3.* In addition, alterations in energy metabolism, behavior and neurological functions were detected in *Scube3*$^{N294K/N294K}$ mice. The *Scube3*$^{N294K/N294K}$ mutant mouse line may serve as a new model for further studying the effect of impaired *SCUBE3* gene function.

INTRODUCTION

The vertebrate Scube (Signal peptide, CUB and EGF-like domain-containing protein) family consists of three independent members Scube1-3. These encode secreted cell surface-associated glycoproteins that share a domain organization of at least five recognizable motifs and the ability to both homo- and heterodimerize (Xavier et al. 2013). Human *SCUBE3* was originally identified following transcriptional profiling of vascular endothelial cells and demonstrated significant enrichment in primary osteoblasts and long bones (Wu et al. 2004). SCUBE3 is a signal protein that is expressed during embryonic development in several tissues (Xavier et al. 2013). In mice, *Scube3* is expressed in ectodermal, endodermal and mesodermal derivatives as also other members of the *Scube* gene family (Haworth et al. 2007). Expression of these genes has been shown to be dynamic and both reciprocal and complementary to each other (Xavier et al. 2013, Haworth et al. 2007).

Although the understanding of the function of *SCUBE3* in embryonic development as well as during adulthood is still marginal, one major function appears to be in bone development and homeostasis and another one in neurological functions. Interestingly, human *SCUBE3* maps to chromosome 6p21.3, a region that has been linked to Paget disease of bone (PDB1) (Fotino et al. 1977, Tilyard et al. 1982), which is characterized by focal areas of increased bone turnover (Ralston et al. 2008). *SCUBE3* function was also associated to other tissues, for example, *Scube3* overexpression in transgenic mice induced cardiac hypertrophy (Yang et al. 2007), and recently, zebrafish Scube3 was identified as a key regulator of fast muscle development by modulating fibroblast growth factor signaling (Tu et al. 2014). Further associations of Scube3 were reported to hedgehog signal transduction (Johnson et

al. 2012), angiogenesis (Yang et al. 2013) and the immune system (Luo et al. 2012). In addition, deregulation of *SCUBE3* was found in different tumor tissues such as lung cancer (Wu et al. 2011, Zhao et al. 2013) or renal carcinomas (Morris et al. 2011).

Although SCUBE3 seems to be involved in many different organ systems and diseases, there is no suitable mouse model so far to study functional alterations. Recent publications on mice lacking *Scube3* did not show any obvious phenotype (Xavier et al. 2010, Xavier et al. 2013). In this study, we present the first *Scube3* mutant mouse line with phenotypic alterations: *Scube3*$^{N294K/N294K}$. The mutant mouse line carries a recessive point mutation in *Scube3* and was derived from the Munich *N*-ethyl-*N*-nitrosourea (ENU) mouse mutagenesis project (MEP, Hrabe de Angelis et al. 2000, Sabrautzki et al. 2012). A systemic phenotypic characterization (Hrabe de Angelis et al. 2015) of this new mutant mouse line annotates *Scube3* gene function in mice to bone metabolism and morphology, renal function, hearing as well as neurological and behavioral functions and energy metabolism.

MATERIAL AND METHODS

Generation of *Scube3*$^{N294K/N294K}$ mutants

ENU mutagenesis and breeding were performed as described on a pure C3HeB/FeJ (C3H) background (Hrabe de Angelis et al. 2000, Sabrautzki et al. 2012, Aigner et al. 2011). Briefly, C3H mice were originally purchased from the Jackson Laboratory (Bar Harbour, Maine) and ENU (Serva Electrophoresis, Heidelberg, Germany) was applied in three weekly intervals by intraperitoneal injections of 90 mg/kg body weight to 10-12 weeks old male mice (G0). G0 mice were mated with wild-type C3H females to produce F1 offspring. F1-males not showing any obvious phenotypic alterations were mated with wild-type C3H females to obtain the G2 generation. We either choose 6-8 female G2 mice for matings with their F1 father or performed intercross matings of G2 mice to produce at least 20 mice (G3 families). Phenotyping for dysmorphological alterations was performed according to a standardized protocol (Fuchs et al. 2000). A mutation was confirmed by showing a Mendelian distribution of expected homozygous mutant mice. The *Scube3*$^{N294K/N294K}$ mouse line was maintained on the C3H genetic background for more than ten generations.

Chromosomal mapping

Homozygous carriers of the G3 generation were mated to C57BL/6J (B6) wild-type mice and the progeny (F1 generation) was intercrossed. DNA was prepared from tail tips of affected offspring (F2 generation). For chromosomal mapping, a microsatellite panel for polymorphic markers between C3H and B6 was used (Hrabe de Angelis et al. 2000).

Whole exome sequencing

For enrichment of exonic sequences we used the SureSelectXT Mouse All Exon 50 Mb kit (Agilent) followed by Illumina HiSeq2000 sequencing as 100 base-pair (bp) paired-end runs with an average 108x coverage (>93% of the target being covered >20x). To search for the causative variants we compared the sequences of one *Scube3*$^{N294K/N294K}$ mouse to one mouse from the C3HeB/FeJ background strain.

Phenotypic analysis

For the phenotypic characterization of young adult (starting in the age of seven weeks) *Scube3*$^{N294K/N294K}$ mutants, a cohort of 15 male and 15 female *Scube3*$^{N294K/N294K}$ mutants as well as 15 male and 15 female wild-type littermate controls (*Scube3*^{WT}) was analyzed in the primary phenotyping screen of the German Mouse Clinic (Hrabe de Angelis et al. 2015, Gailus-Durner et al. 2005, Fuchs et al. 2012, Fuchs et al. 2011). The tests within the phenotyping pipeline and the corresponding age of the animals, as well as references for the protocols are shown in Table S1. For further detailed investigation of observed phenotypes, secondary tests were carried out. Details for the applied protocols are listed below.

Progression study

Since *Scube3*$^{N294K/N294K}$ mice showed signs of an impaired bone metabolism, we tested groups of *Scube3*$^{N294K/N294K}$ and *Scube3*^{WT} mice at 12, 24, 36 and 52 weeks of age for the clinical chemical plasma parameters inorganic calcium (Ca), total inorganic phosphate (P_i), total alkaline phosphatase (ALP), cholesterol (CHO), triglycerides (TGL), glucose (GLUC), total protein (TP), urea (U), uric acid (UA) and

albumin (ALB) by using an AU480 clinical chemistry analyzer (Beckman-Coulter, Krefeld, Germany) and adapted reagent kits provided by Beckman-Coulter. Additionally, pQCT (peripheral Quantitative Computed Tomography, Stratec, Pforzheim, Germany) analyses of the femoral metaphysis and diaphysis were performed at the age of nine and twelve months. We measured CTX-1 in plasma of 52 weeks old mice using RatLaps (carboxy-terminal collagen crosslinks, CTX-1) EIA ELISA from IDS (Frankfurt am Main, Germany) according to the manufacturer's protocol.

Analysis of renal function in metabolic cages

A subgroup of 48 animals (12 mutant and control mice each of both sexes) at the age of 34 weeks was subjected to a renal function test using metabolic cages for single mice (Tecniplast, Buguggiate, Italy) to collect 48-hour urine samples and monitor water and urine production. During the test, mice had free access to water and pulverized food. Tests were conducted as described previously starting with a single blood sample collection followed by urine collection over 48 hours (Fuchs et al. 2011). Urine and plasma samples were analyzed for a set of 12 clinical chemistry parameters including concentrations of sodium, potassium and chloride (Na, K, Cl), Ca, P_i, creatinine (Crea), U, UA, GLUC as well as TP and ALB, as described above.

Transcriptome analysis

Transcriptome analyses from kidney samples of four *Scube3*$^{N294K/N294K}$ and four *Scube3*^{WT} male mice at the age of 29 weeks were performed following total RNA extraction (RNAeasy Midi kit, Qiagen). Illumina Mouse Ref8 v2.0 Expression BeadChips were employed as previously described (Horsch et al. 2008, Kugler et al.

2013). Illumina Genomestudio 2011.1 was used for data normalization (cubic spline) and statistical analysis for the identification of differential gene expression was performed with SAM (Significant Analysis of Microarrays, fold change > 1.6, FDR < 6%) (Saeed et al. 2006, Tusher et al. 2001). Overrepresented functional annotations were obtained through the use of QIAGEN's Ingenuity Pathway Analysis (IPA®, QIAGEN Redwood City, www.qiagen.com/ingenuity). Expression data are available at the GEO database under GSE56402.

Inner ear preparation

Inner ears were dissected from the temporal bones of sacrificed animals and fixed in 4% formalin (Carl Roth GmbH, Karlsruhe, Germany). Following dehydration in ethanol, inner ears were immersed in methyl salicylate (Sigma Aldrich, Taufkirchen, Germany) and incubated overnight. Analysis of cleared inner ears was documented by photographic images.

Feces analysis

Fecal samples were collected in single caged mice for five consecutive days. Feces were separated from other material (bedding, food), desiccated in a drying oven at 60°C until weight constancy before bomb calorimetric combustion (IKA C7000, Staufen, Germany). Calorie content of food samples was also determined by bomb calorimetry. Energy uptake was calculated by multiplying food energy content and total amount of food consumed. Egested energy was calculated from feces energy content multiplied by amount of egested feces (see also Rozman et al. 2014).

Statistical analysis

The Shapiro Wilk test as well as histograms and quantile-quantile plots were used to assess the normality of the investigated parameters. For continuous data meeting the assumption of normality, a two-way ANOVA with a Tukey HSD post hoc test or a linear model (including body weight as an additional covariate in some cases) was performed to test genotype-sex interaction effects. In tables, normally distributed data were expressed as means ± standard deviations. Parameters with a skewed distribution were analyzed using the nonparametric Wilcoxon rank sum test and were presented as median as well as 25th percentile and 75th percentile in the tables. Categorical parameters were analyzed by a Fisher's exact test and are presented as absolute numbers. For all tests, a P value < 0.05 was used as level of significance. Since the primary phenotyping screen in the German Mouse Clinic was mainly designed as a high-throughput screening for new phenotypic alterations, a correction for multiple testing of the various parameters was not performed. Data were analyzed using R software (Version 3.0.2; Foundation of Statistical Computing, Vienna, Austria).

Housing and handling of mice was according to the German Animal Welfare Act. The animal experiments were approved by the Government of Upper Bavaria (112-02, 78-06, 144-10, 126-11).

Data availability

Data of the complete phenotypic assessment is accessible via the website of the German Mouse Clinic (www.mouseclinic.de/ phenomap/jsp/annotation/public/phenomap.jsf), and the *Scube3*$^{N294K/N294K}$ mutant

mouse line is accessible via the European Mouse Mutant Archive (EMMA, www.infrafrontier.eu) under EMMA ID EM:10872.

RESULTS

Generation of *Scube3*$^{N294K/N294K}$ mice

The *Scube3*$^{N294K/N294K}$ mutation was generated in the large-scale Munich ENU mutagenesis program. The mutant line was identified by screening G3 animals for morphological abnormalities resulting in reduced body size (figure 1A), a shorter and kinky tail, abnormal digit positioning and an abnormal posture when hung by the tail. *Scube3*$^{N294K/N294K}$ variants were crossed to wild-type C3HeB/FeJ (C3H) mice, and none of the offspring showed the characteristic *Scube3*$^{N294K/N294K}$ phenotypes. However, intercrossing these heterozygous mice resulted in a fraction of about 25% of offspring that showed the characteristic *Scube3*$^{N294K/N294K}$ phenotypes. We therefore considered *Scube3*$^{N294K/N294K}$ a recessive mutant mouse line, and maintained the mutation on a pure C3H genetic background for more than ten generations.

Mutation detection

Rough mapping by an out-cross/inter-cross breeding strategy with C57BL/6J (B6) animals revealed a 12.4 Mb critical region on chromosome 17 between markers D17Mit46 and D17Mit34 with no recombinants near marker D17Mit198. Whole exome sequencing identified a homozygous non-synonymous sequence variation within the *Scube3* gene, the only candidate gene within the critical region on chromosome 17. A C to A transversion at nucleotide position 882 in exon 8 of *Scube3* leads to an asparagine to lysine exchange at protein position 294 (N294K). This non-synonymous sequence variation co-segregated with the *Scube3*$^{N294K/N294K}$ phenotype in all 15 tested mutant mice and was not confirmed in 10 wild-type

littermates and other mice of inbred C3H, BALB/c, and B6 strains. Subsequently, this mutation was confirmed in more than one hundred mutant *Scube3*$^{N294K/N294K}$ mice during maintenance breeding and excluded in the equal number of wild-type littermates.

The N294K substitution is located within the calcium-binding EGF-like domain 7 of SCUBE3, which is highly conserved between mice, human, zebrafish and chicken (data not shown). Using the protein prediction programs PROVEAN (http://provean.jcvi.org; Choi et al. 2012) and PolyPhen-2 (http://genetics.bwh.harvard.edu/pph2) this sequence variation was classified as deleterious or probably damaging with a score of 0.99.

Phenotypic analysis

A cohort of 15 male and 15 female *Scube3*$^{N294K/N294K}$ mice and the respective number of *Scube3*^{WT} mice were analyzed in the German Mouse Clinic in the screens for behavior, neurology, nociception, vision and eye, dysmorphology, bone and cartilage, energy metabolism, hematology, clinical chemistry, steroid metabolism, immunology, allergy, cardiovascular system, lung function, molecular phenotyping and pathology.

Scube3$^{N294K/N294K}$ *mice show skeletal abnormalities and changes in bone metabolism*

In addition to the afore mentioned smaller body size, shorter and kinked tails and abnormal digit positioning, X-ray analysis of the skeleton showed no obvious craniofacial abnormalities but detected malformations of the thoracic and lumbar vertebrae, and shorter femora (figure 1A, Table S2C) in *Scube3*$^{N294K/N294K}$ mice that were independent of the body size reduction. Rib fusions occurred with low penetrance (3% of observed animals, data not shown). In DEXA analysis, bone

mineral density (BMD) and bone mineral content (BMC) were significantly decreased (Table S2B), but the results might be confounded by body weight (figure 1B and C). Several parameters in pQCT-measurements supported the findings of the DEXA analysis. The effects were weaker in 12 months old than in nine months old mice (Table S3).

Calcium levels at the age of 17 weeks were elevated in *Scube3*$^{N294K/N294K}$ female mice but this finding was not confirmed in older animals. P_i levels were globally decreased in male mice and ALP activities in mice of both sexes were increased with effects getting weaker with age. At one year of age, *Scube3*$^{N294K/N294K}$ mice showed a significant increase of the bone resorption marker CTX-1 (figure 2).

Scube3$^{N294K/N294K}$ *mice have defects in bone growth, but not in embryonic patterning*

For further investigation of the observed bone abnormalities we analyzed *Scube3*$^{N294K/N294K}$ mice at newborn and various embryonic stages by skeletal staining. Multiple hyper-ossifications in the axial and appendicular skeleton were detected. In thoracic, lumbar, and sacral vertebrae of *Scube3*$^{N294K/N294K}$ mice, ossification center and pedicles were more closed and fused compared to those of wild type mice (figure 3B, asterisks indicate the ossification center). Further, in some thoracic vertebrae ossification centers were split in mutant mice (figure 3B, two asterisks in one vertebrae). In the appendicular skeleton, the coracoid processes showed hyper-ossification, and proximal and middle phalanges in digit II started to be fused (figure 3F, arrowhead and black asterisks). Furthermore, metacarpal, metatarsal and tarsal were enlarged due to hyper-ossification (figure 3F and 3H, white asterisks). These hyper-ossification phenotypes were not detected at embryonic day E15.5 around the time when endochondral ossification starts, but

were detected in E17.5 *Scube3*$^{N294K/N294K}$ embryos (data not shown), suggesting that malformations of *Scube3*$^{N294K/N294K}$ mice are due to defects in bone growth, but not because of disturbed embryonic patterning as in vertebral segmentation disorders.

Scube3$^{N294K/N294K}$ *mice show symptoms pointing to disturbances in renal function*

Urea, creatinine and potassium levels as well as alpha-amylase activities were increased in plasma of *Scube3*$^{N294K/N294K}$ mice of both sexes (Table S2B). The findings were consistent for most parameters over the whole life period (measured at 12, 24, 36 and 52 weeks of age, figure 2). In addition, plasma glucose levels, triglyceride and P_i concentrations were decreased in both sexes, whereas total protein, albumin and cholesterol were decreased only in male mutants (Table S2B). To follow up these findings, we analyzed renal function in metabolic cages. Calculated 24h creatinine clearance adjusted to body weight was normal in *Scube3*$^{N294K/N294K}$ mice, suggesting that a similar amount of plasma was filtered per g body mass by the kidneys of mutant and control mice within 24 hours (Table 1). However, water uptake and urine production in relation to body mass (Table 1) as well as food consumption (2.85 ± 0.23 vs. 2.02 ± 0.35 and 3.18 ± 0.57 vs. 2.64 ± 0.47 g/24h in mutant vs. control males and females, respectively) were significantly higher in *Scube3*$^{N294K/N294K}$ mice. Urinary concentrations of electrolytes and urea were comparable, while creatinine, protein (total protein and albumin) as well as glucose concentrations were slightly lower and uric acid level was significantly lower in *Scube3*$^{N294K/N294K}$ mice (data not shown). In consequence, calculated 24h excretion values per 25g body mass and fractional excretion rates were significantly increased in *Scube3*$^{N294K/N294K}$ mice for the electrolytes Na, K, Cl, as well as Ca, urea, total protein, albumin and glucose. Uric acid and phosphate excretion adjusted to body

mass was found to be highly variable and did not significantly differ between genotypes (Table 1).

Transcriptome analysis suggests a role of Scube3 in reabsorption and/or excretion of urine components

We performed transcriptome analysis of kidney samples from *Scube3*$^{N294K/N294K}$ mice. Statistical analysis of gene expression patterns identified 138 differentially expressed genes functionally classified by the following overrepresented terms: cellular development, movement and proliferation, as well as cardiovascular system function, developmental disorder and renal and urological disease (Table 2). Additionally, literature based research revealed several genes associated with expression in proximal tubules (*Havcr1, Has2, Met, Mep1b, Mme* and *Slc29a8*), reabsorption of electrolytes (proximal tubule epithelium: *Cldn10* and *Slc12a1*) and maintenance of salt/water balance of blood (renal medulla: *Acta2*, *Adamts1*, *Ehd3*, *Kcnj15* and *Umod*). All these genes were down-regulated in kidney.

Scube3$^{N294K/N294K}$ *mice have hearing deficits, alterations in the inner and middle ear and show behavioral abnormalities*

Hearing sensitivity was assessed by auditory brainstem response (ABR) to different auditory stimuli. There were significant differences at clicks and all tested frequencies: thresholds were increased in *Scube3*$^{N294K/N294K}$ mice of both sexes, with female *Scube3*$^{N294K/N294K}$ mice more severely affected (figure 4A). Further analysis of this finding revealed alterations in inner and middle ear preparations. The inner and middle ears appeared smaller and the ossicles of the middle ear had decreased size and altered shape. The incus was smaller and especially body and head of the

malleus was decreased in size (figure 4B). The middle ear cavity, the bulla, part of the temporal bone, had an irregular shape as well (figure 4B).

In the open field test, *Scube3*$^{N294K/N294K}$ mice showed clearly decreased locomotor and exploratory activity as indexed by a reduction in total distance travelled and rearing activity over the course of the 20-minute test. Movement velocity was also decreased. In terms of anxiety-related behavior, *Scube3*$^{N294K/N294K}$ mice spent less time in the center, entered into the center less often, travelled less distance within this zone and exhibited an increased latency to enter the center (figure 5, Table S2B). In the modified hole-board test, maximum and angular velocity were decreased in *Scube3*$^{N294K/N294K}$ mice as well as the latency to engage in risk assessment by the male mutant mice (Table S2B).

In a general observation series according to the modified SHIRPA protocol, we also observed reduced locomotor activity, particularly in female *Scube3*$^{N294K/N294K}$ mice. In addition, we found a reduction in grip strength, which was also influenced by the body mass reduction (Table S2B and C, figure 5).

Scube3$^{N294K/N294K}$ *mice have altered function in energy metabolism*

Scube3$^{N294K/N294K}$ mice had significantly reduced body mass, and considerably lower absolute fat and lean mass (Table S2C). They also showed a significant shift in body composition in particular with decreased lean mass when adjusted to body mass (figure 6). Interestingly, the relations between body mass and fat content, as well as body mass and lean mass were significantly different between genotypes (Table S2C), indicating a systematic effect on body composition. *Scube3*$^{N294K/N294K}$ mice had significantly lower glucose, triglyceride, NEFA and glycerol concentrations in plasma, (Table S2B). In the glucose tolerance test, basal fasting glucose levels were

significantly decreased in *Scube3*$^{N294K/N294K}$ mice. AUC (area under the curve) values were decreased, which indicates an improved glucose tolerance in *Scube3*$^{N294K/N294K}$ mice (Table S2B). We applied indirect calorimetry to investigate energy expenditure, substrate use and locomotor activity under home-cage conditions, and found rearing behavior decreased during the 21 hours test phase. No major effects on energy turnover could be detected when VO2 was adjusted to body mass (Table S2C). In a separate test, food consumption and gastro-intestinal functions of *Scube3*$^{N294K/N294K}$ mice were monitored over five days in single caged animals. We could not detect considerable effects on food intake, energy assimilation, and the efficiency of energy extraction from food.

Scube3$^{N294K/N294K}$ *mice show mild alterations in cardiovascular parameters, but no hints for deficits in heart performance or conduction*

Echocardiography and electrocardiography revealed several mild alterations in *Scube3*$^{N294K/N294K}$ mice (decreased interventricular septum width, decreased left ventricular posterior wall thickness, decreased left ventricular mass and prolonged QRS interval duration mainly in male *Scube3*$^{N294K/N294K}$ mice, as well as decreased diastolic ventricular dimension and decreased respiration rate in female *Scube3*$^{N294K/N294K}$ mice, Table S2A). We found a significantly lower heart weight of *Scube3*$^{N294K/N294K}$ mice as compared to sex-matched controls (also when normalized to tibia length). However, no alterations were found in heart performance or conduction and thus there was no clear hint for a physiologically relevant constraint of cardiovascular function due to the mutation. Further in line, the observed alterations may be confounded by the reduced body weight of *Scube3*$^{N294K/N294K}$ mice.

Further tested organ functions are normal in Scube3$^{N294K/N294K}$ mice

The analysis of immunologically relevant parameters revealed no major changes. We observed tendencies towards decreased L-selectin expressing cells within T cell populations and increased frequency of CD11b expressing cells within the NK cell compartment (Table S2A). We did not detect any changes in hematological parameters. Eye morphology and vision were as expected for the genetic background (C3HeB/FeJ). There were no major genotype effects on prepulse inhibition responding or pain perception. No differences were detected for rotarod performance. The analysis of trans-epidermal water loss (TEWL) from the skin of the mice did not reveal genotype-specific differences as well as hair structure and coat appeared normal. There were no alterations in lung function. *Scube3$^{N294K/N294K}$* mice at the age of 21 weeks did not present additional histopathological alterations.

DISCUSSION

We identified an ENU-derived mouse line carrying a missense mutation in *Scube3* (NM_001004366.1:c.882C>A, NP_001004366.1:p.Asn294Lys), and characterized the *Scube3*$^{N294K/N294K}$ mutant mouse in detail in the German Mouse Clinic (Hrabe de Angelis et al. 2015, Gailus-Durner et al. 2005, Fuchs et al. 2012). As shown previously in a *Scube3* reporter mouse line, targeted replacement of exons 2 and 3 by a *lacZ*-cassette demonstrated early expression of the gene in craniofacial, limb and neural tube tissues (Xavier et al. 2010). However, these mice as well as SCUBE3 loss-of-function mice developed normally and did not show overt phenotypic alterations (Xavier et al. 2013, Xavier et al. 2010) whereas *Scube3*$^{N294K/N294K}$ mice exhibited alterations in several organ systems. One reason for this discrepancy might be owed to the different genetic backgrounds of the mice in these studies. However, a more likely explanation is the redundancy of *Scube* family members, which might compensate the loss of SCUBE3 in the null mutant (Xavier et al. 2013), and the nature of the mutation in the *Scube3* mouse model described here. The amino-acid exchange in *Scube3*$^{N294K/N294K}$ mice lies within the EGF-like domain 7 that follows the consensus sequence D/N-X-D/N-E/Q-X_m-D/N*-X_n-Y/F for calcium-binding EGF-like domains (cbEGFs, figure 7). These domains are known to mediate protein-protein and protein-carbohydrate interactions in a calcium-dependent manner (Downing et al. 1996). They are also structurally important for several cellular processes such as extracellular matrix architecture or specification of cell fates (Downing et al. 1996). For example, missense mutation of conserved amino acids in cbEGFs of fibrillin 1 (FBN1) are causative for Marfan syndrome due to Ca^{2+}-dependent misfolding of the protein (Whiteman et al. 2007). Likewise, the amino-acid

exchange in the cbEGF domain 7 in *Scube3*$^{N294K/N294K}$ mice might lead to a reduced Ca^{2+}-binding capacity and/or to conformational changes, which in turn could negatively interfere with both homo- and heteromeric interaction of SCUBE proteins (Wu et al. 2004, Yang et al. 2002), posttranslational processing (Wu et al. 2011) and interaction with transforming growth factor-β and hedgehog signaling (Johnson et al. 2012, Wu et al. 2011).

Scube3 is expressed in the cartilaginous primordia of the skeleton and regions of intramembranous bone formation in the developing craniofacial region (Haworth et al. 2007). Nevertheless, besides middle ear abnormalities, *Scube3*$^{N294K/N294K}$ mice did not show any further craniofacial abnormalities suggesting that SCUBE3 is dispensable for craniofacial development (Xavier et al. 2013) or the respective functions may be assigned to regions upstream of cbEGF7 of SCUBE3. However, the *Scube3*$^{N294K/N294K}$ mutation directly affects bone morphology and bone metabolism. *Scube3*$^{N294K/N294K}$ mice had a significant reduction in body size and weight. Interestingly, GWAS found *SCUBE3* SNPs among adult and pediatric height associated loci (Gudbjartsson et al. 2008, Zhao et al. 2010) as well as in pigs associated with body height, body length and rump circumference (Wang et al. 2014). The influence of the *Scube3* mutation on bone metabolism was expressed by increased ALP activities and CTX-1 values in plasma, as well as by decreased bone mineral density and bone mineral content in DEXA and pQCT analysis. These data are supported by the finding that SCUBE3 is expressed in early osteoblasts and long bones (Wu et al. 2004). Interestingly, the human *SCUBE3* gene is located on chromosome 6p21.3, which was discussed to be associated with Paget disease of bone (PDB1) (Wu et al. 2004, Fotino et al. 1977, Tilyard et al. 1982, Good et al. 2002). Although Paget disease of bone (PDB) is characterized by late onset and

mostly focal bone abnormalities due to increased bone turnover (Ralston et al. 2008), mouse models for genes known to be mutated in PDB such as *Tnfrsf11a* for PDB2 (OMIM 603499) and *Sqstm1* for PDB3 (OMIM 601530) have bone abnormalities already at birth (Dougall et al. 1999, Li et al. 2000) or not until adulthood (Kapur et al. 2004, Durán et al. 2004, Daroszewska et al. 2011). Interestingly, cases of PDB were described to be associated with raised ALP activities and deafness (Tan et al. 2014). We therefore suggest *Scube3*$^{N294K/N294K}$ mice as a new model for further studies on PDB1.

SCUBE3 maps to a region that was associated with progressive bilateral hearing loss of the mid and high frequencies (DFNA31, OMIM %608645) (Snoeckx et al. 2004). The results of the ABR-hearing assessment and the morphological analysis of the middle ears of *Scube3*$^{N294K/N294K}$ animals indicate conductive hearing loss. In *Scube3*$^{N294K/N294K}$ mice, hearing loss might be a consequence of retarded development of middle ear cavity and ossicle malformations. By contrast, Xavier et al. (2013) did not observe any gross abnormalities in the (inner) ears of *Scube3*$^{-/-}$ mice at the age of E17.5. Since background-specific genetic modifiers play an important role in the development of inner ears (Kiernan et al. 2007) the differences in the genetic background could be the reason for the different observations in the two studies.

The kidneys play a central role in regulation of mineral homeostasis and chronic kidney disease (CKD) is associated with bone metabolic disease. However, the regulatory pathways involved are still not fully understood (reviewed in Hu et al. 2013, Peacock 2010, Razzaque 2011, Rowe 2012). Elevated plasma urea and creatinine levels found in *Scube3*$^{N294K/N294K}$ mice hint towards possible effects on renal function. We found increased electrolyte and water excretion, but no alteration

of creatinine clearance. These findings could be a sign of altered renal tubular function or might be a consequence of increased electrolyte consumption due to higher food uptake causing an upregulation of excretory mechanisms. The annotations of differentially expressed genes in kidney with reabsorption of electrolytes and salt/water balance indicate effects on tubular reabsorption. *Acta2* (Tanabe et al. 2012), *Adamts1* (Schrimpf et al. 2012), *Ehd3* (George et al. 2011), *Kcnj15* (Derst et al. 1998) and *Umod* (Rampoldi et al. 2011) are annotated with expression in renal medulla and salt/water balance and *Clnd10* (Kung et al. 2012), *Havcr1* (Adivanti and Loho 2012), *Has2* (Michael et al. 2011), *Mep1b* (Oneda et al. 2008), *Met* (Zhou et al. 2013), *Mme* (Van der Hauwaert et al. 2013), Slc12a1 (Yang et al. 1996) and *Slc39a8* (Nebert et al. 2012) are associated with electrolyte reabsorption in the proximal tubules. Together these findings hint towards a possible role of *Scube3* in kidney development and function, supported by the expression of *Scube3* in the developing kidney (Haworth et al. 2007), or might be related to secondary effects on the regulation of kidney function.

The human SCUBE3 protein is involved in hedgehog and TGF-β1 signaling (Xavier et al. 2013, Haworth et al. 2007, Yang et al. 2007, Johnson et al. 2012) but, so far, nothing is known about SCUBE3 signaling in this network in mice. Transcriptome profiling analysis of kidney from *Scube3*$^{N294K/N294K}$ mice identified potential down-stream targets of SCUBE3 that are annotated to TGF-β1 signaling (*C1qtnf3* (Hofmann et al. 2011), *Foxc1* (Xu et al. 2012), *Has2* (Davies et al. 2005), *Jdp2* (Mito et al. 2013), *Kcnip2* (Kaur et al. 2013), *Lefty2* (Saijoh et al. 2000, Arganaraz et al. 2012), *Tgfbr3* (Walker et al. 2011), and *Tnn* (Alejandre Alcázar et al. 2011)). Reduced expression of all these genes give evidence for a supportive role of

SCUBE3 within the TGF-β1 signaling pathway by binding to transforming growth factor beta receptor 2 (TGFBR2) (Yang et al. 2007).

Although we did not observe structural defects of muscle tissue in the pathological examination, the repeated findings of reduced locomotor and rearing activity as well as movement velocity might be indications for functional defects, which might also be associated with an abnormal muscle energy metabolism. Indeed, very recent findings by detailed analysis of zebrafish *scube3* suggest that its gene function is crucial for fast-fiber myogenesis (Tu et al. 2014). Still, decreased activity and movement velocity could also be due to the described early developmental expression of *Scube3* in the neural tube (Haworth et al. 2007).

SCUBE3 expression was observed in human cultured coronary smooth muscle cells and at low levels in the heart (Wu et al. 2004) and its overexpression led to cardiac hypertrophy in transgenic mice (Yang et al. 2007). Whereas young *Scube3* transgenic mice appeared phenotypically normal but showed abnormal repolarization ECG patterns as well as thickening of left-ventricular septum and posterior wall thickness when analyzed at 8 months of age (Yang et al. 2007), $Scube3^{N294K/N294K}$ mice showed only very mild alterations in cardiac parameters of our phenotypic analysis. Possibly, they were too young for manifestation of a severe cardiac dysfunction.

In this study, we characterized the first *Scube3* mutant mouse line with phenotypic alterations, suggesting a role of *Scube3* in bone metabolism and morphology, hearing and renal function. The observed morphological abnormalities of the skeleton, impaired bone metabolism and hearing impairments correlate with the rare metabolic bone disorder Paget disease of bone (PDB), associated with the

chromosomal region of human SCUBE3. Further phenotypic alterations were observed in energy metabolism parameters, in behavior and neurological functions (figure 7). This new mouse model helps to better understand SCUBE3 function and diseases related to *Scube3* gene mutations.

ACKNOWLEDGEMENTS

We want to thank Andreas Mayer, Sandra Hoffmann, Gerlinde Bergter, Silvia Crowley, Reinhard Seeliger, Jan Einicke, Michael Färberböck, Daniel Feeser, Ralf Fischer, Anna Fuchs, Corinne Graf, Brigitte Herrmann, Christine Hollauer, Elfi Holupirek, Sebastian Kaidel, Maria Kugler, Sören Kundt, Sandy Lösecke, Jacqueline Müller, Anna Nießer, Elenore Samson, Florian Schleicher, Ann-Elisabeth, Schwarz, Nadine Senger, Verena Simion, Yvonne Sonntag, Bettina Sperling, Lucie Thurmann, Susanne Wittich, Julia Wittmann, and Anja Wohlbier for expert technical help as well as Horst Wenig, Manuela Huber, Tina Reichelt, Michael Gerstlauer, Heidi Marr, Annica Miedl, Renate Huber and Richard Klein for the care of the mice. We thank Dr. Elisabeth Grundner-Culemann for project discussions and Dr. Robert Brommage for helpful discussion and careful revision of the manuscript.

This work was supported by the German Federal Ministry of Education and Research to the GMC (Infrafrontier grant 01KX1012), the German Center for Diabetes Research (DZD), BMBF OSTEOPATH grants (01EC1006B), the German Center for Vertigo and Balance Disorders (grant 01EO 0901), by the Helmholtz Alliance for Mental Health in Ageing Society (HA-215) and by the DFG grant 'DJ-1 Linked Neurodegeneration Pathways in New Mouse Models of Parkinson's Disease' (WU 164/5-1).This work was partially supported by grants from the Helmholtz Portfolio Theme 'Metabolic Dysfunction and Common Disease', and the Helmholtz Alliance 'Imaging and Curing Environmental Metabolic Diseases, ICEMED'.

Conflict of interest

The authors declare that there are no conflicts of interest

REFERENCES

Adiyanti, S. S., and T. Loho, 2012 Acute Kidney Injury (AKI) biomarker. Acta Med. Indones., 44, 246-55.

Aigner, B., B. Rathkolb, M. Klempt, S. Wagner, D. Michel *et al.*, 2011 Generation of N-ethyl-N-nitrosourea-induced mouse mutants with deviations in hematological parameters. Mamm. Genome, 22, 495-505.

Alejandre Alcázar, M. A., R. E. Morty, L. Lendzian, C. Vohlen, I. Oestreicher *et al.*, 2011 Inhibition of TGF-beta signaling and decreased apoptosis in IUGR-associated lung disease in rats. PLoS One, 6; e26371.

Arganaraz, M. E., S. A. Apichela, and D. C. Miceli, 2012 LEFTY2 expression and localization in rat oviduct during early pregnancy. Zygote, 20, 53-60.

Choi, Y., G. E. Sims, S. Murphy, J. R. Miller, and A. P. Chan, 2012 Predicting the functional effect of amino acid substitutions and indels. PLoS One, 7, e46688.

Daroszewska, A., R. J. van 't Hof, J. A. Rojas, R. Layfield, E. Landao-Basonga *et al.*, 2011 A point mutation in the ubiquitin-associated domain of SQSMT1 is sufficient to cause a Paget's disease-like disorder in mice. Hum. Mol. Genet., 20, 2734-2744.

Davies, M., M. Robinson, E. Smith, S. Huntley, S. Prime *et al.*, 2005 Induction of an epithelial to mesenchymal transition in human immortal and malignant keratinocytes

by TGF-beta1 involves MAPK, Smad and AP-1 signalling pathways. J. Cell. Biochem., 95, 918-931.

Derst, C., E. Wischmeyer, R. Preisig-Müller, A. Spauschus, M. Konrad *et al.*, 1998 A hyperprostaglandin E syndrome mutation in Kir1.1 (renal outer medullary potassium) channels reveals a crucial residue for channel function in Kir1.3 channels. J. Biol. Chem., 273, 23884-23891.

Dougall, W. C., M. Glaccum, K. Charrier, K. Rohrbach, K. Brasel *et al.*, 1999 RANK is essential for osteoclast and lymph node development. Genes Dev., 13, 2412-2424.

Downing, A. K., V. Knott, J. M. Werner, C. M. Cardy, I. D. Campbell *et al.*, 1996 Solution Structure of a Pair of Calcium-Binding Epidermal Growth Factor-like Domains: Implications for the Marfan Syndrome and Other Genetic Disorders. Cell, 85, 597-605.

Durán, A., M. Serrano, M. Leitges, J. M. Flores, S. Picard *et al.*, 2004 The atypical PKC-interacting protein p62 is an important mediator of RANK-activated osteoclastogenesis. Dev. Cell., 6, 303-309.

Fotino, M., A. Haymovits, and C. T. Falk, 1977 Evidence for linkage between HLA and Paget's disease. Transplant. Proc., 9, 1867-1868.

Fuchs, H., K. Schughart, E. Wolf, R. Balling, and M. Hrabé de Angelis, 2000 Screening for dysmorphological abnormalities--a powerful tool to isolate new mouse mutants. Mamm. Genome, 11, 528-30.

Fuchs, H., V. Gailus-Durner, T. Adler, J. A. Aguilar-Pimentel, L. Becker *et al.*, 2011 Mouse phenotyping. Methods, 53, 120-135.

Fuchs, H., V. Gailus-Durner, S. Neschen, T. Adler, L. C. Afonso *et al.*, 2012 Innovations in phenotyping of mouse models in the German Mouse Clinic. Mamm. Genome, 23, 611-22.

Gailus-Durner, V., H. Fuchs, L. Becker, I. Bolle, M. Brielmeier *et al.*, 2005 Introducing the German Mouse Clinic: open access platform for standardized phenotyping. Nat. Methods, 2, 403-404.

George, M., M. A. Rainey, M. Naramura, K. W. Foster, M. S. Holzapfel *et al.*, 2011 Renal thrombotic microangiopathy in mice with combined deletion of endocytic recycling regulators EHD3 and EHD4. PLoS One, 6, e17838.

Good, D. A., F. Busfield, B. H. Fletcher, D. L. Duffy, J. B. Kesting *et al.*, 2002 Linkage of Paget disease of bone to a novel region of human chromosome 18q23. Am. J. Hum. Genet., 70, 517-525.

Gudbjartsson, D. F., G. B. Walters, G. Thorleifsson, H. Stefansson, B. V. Halldorsson *et al.*, 2008 Many sequence variants affecting diversity of adult human height. Nat. Genet., 40, 609-615.

Haworth, K., F. Smith, M. Zoupa, M. Seppala, P. T. Sharpe *et al.*, 2007 Expression of the Scube3 epidermal growth factor-related gene during early embryonic development in the mouse. Gene Expression Patterns, 7, 630-634.

Hofmann, C., N. Chen, F. Obermeier, G. Paul, C. Büchler *et al.*, 2011 C1q/TNF-related protein-3 (CTRP-3) is secreted by visceral adipose tissue and exerts antiinflammatory and antifibrotic effects in primary human colonic fibroblasts. Inflamm. Bowel. Dis., 17, 2462-2471.

Horsch, M., S. Schädler, V. Gailus-Durner, H. Fuchs, H. Meyer *et al.*, 2008 Systematic gene expression profiling of mouse model series reveals coexpressed genes. Proteomics, 8, 1248-1256.

Hrabé de Angelis, M., H. Flaswinkel, H. Fuchs, B. Rathkolb, D. Soewarto *et al.*, 2000 Genome-wide, large-scale production of mutant mice by ENU mutagenesis. Nat. Genet., 25,444-447.

Hrabe de Angelis, M., G. Nicholson, M. Selloum, J. K. White, H. Morgan *et al.*, 2015 Analysis of mammalian gene function through broad-based phenotypic screens across a consortium of mouse clinics. Nat. Genet., 47, 969-978.

Hu, M. C., M. Kuro-o, and O. W. Moe, 2013 Renal and extrarenal actions of Klotho. Semin. Nephrol., 33,118-129.

Johnson, J. L., T. E. Hall, J. M. Dyson, C. Sonntag, K. Ayers *et al.*, 2012 Scube activity is necessary for Hedgehog signal transduction in vivo. Dev. Biol., 368,193-202.

Kapur, R. P., Z. Yao, M. H. Iida, C. M. Clarke, B. Doggett *et al.*, 2004 Malignant autosomal recessive osteopetrosis caused caused by spontaneous mutation of murine Rank. J. Bone Miner. Res., 19, 1689-1697.

Kaur, K., M. Zarzoso, D. Ponce-Balbuena, G. Guerrero-Serna, L. Hou *et al.*, 2013 TGF-beta1, released by myofibroblasts, differentially regulates transcription and function of sodium and potassium channels in adult rat ventricular myocytes. PLoS One, 8, e55391.

Kiernan, A. E., R. Li, N. L. Hawes, G. A. Churchill, and T. Gridley, 2007 Genetic background modifies inner ear and eye phenotypes of jag1 heterozygous mice. Genetics. 7, 307-311.

Krug, S. M., D. Günzel, M. P. Conrad, I. F. Lee s. Amasheh *et al.*, 2012 Charge-selective claudin channels. Ann. N. Y. Acad. Sci., 1257, 20-28.

Kugler, J. E., M. Horsch, D. Huang, T. Furusawa, M. Rochman *et al.*, 2013 High mobility group N proteins modulate the fidelity of the cellular transcriptional profile in a tissue- and variant-specific manner. J. Biol. Chem., 288, 16690-16703.

Li, J., I. Sarosi, X. Q. Yan, S. Morony, C. Capparelli *et al.*, 2000 RANK is the intrinsic hematopoietic cell surface receptor that controls osteoclastigenesis and regulation of bone mass and calcium metabolism. Proc. Natl. Acad. Sci. USA, 97, 1566-1571.

Luo, W., S. Chen, D. Cheng, L. Wang, Y. Li *et al.*, 2012 Genome-wide association study of porcine hematological parameters in a Large White × Minzhu F2 resource population. Int. J. Biol. Sci., 8, 870-881.

Michael, D. R., A. O. Phillips, A. Krupa, J. Martin, J. E. Redman *et al.*, 2011 The human hyaluronan synthase 2 (HAS2) gene and its natural antisense RNA exhibit coordinated expression in the renal proximal tubular epithelial cell. J. Biol. Chem., 286, 19523-19532.

Mito, T., K. Yoshioka, M. Noguchi, S. Yamashita, and H. Hoshi, 2013 Recombinant human follicle-stimulating hormone and transforming growth factor-alpha enhance in vitro maturation of porcine oocytes. Mol. Reprod. Dev., 80, 549-560.

Morris, M. R., C. J. Ricketts, D. Gentle, F. McRonald, N. Carli *et al.*, 2011. Genome-wide methylation analysis identifies epigenetically inactivated candidate tumour suppressor genes in renal cell carcinoma. Oncogene, 30,1390-401.

Nebert, D. W., M. Gálvez-Peralta, E. B. Hay, H. Li, E. Johansson *et al.*, 2012 ZIP14 and ZIP8 zinc/bicarbonate symporters in Xenopus oocytes: characterization of metal uptake and inhibition. Metallomics, 4, 1218-1225.

Oneda, B., N. Lods, D. Lottaz, C. Becker-Pauly, W. Stöcker *et al.*, 2008 Metalloprotease meprin beta in rat kidney: glomerular localization and differential expression in glomerulonephritis. PLoS One, 3, e2278.

Peacock, M., 2010 Calcium metabolism in health and disease. Clin. J. Am. Soc. Nephrol., 5 Suppl 1, S23-30.

Ralston, S. H., A. L. Langston, and I. R. Reid, 2008 Pathogenesis and management of Paget's disease of bone. Lancet, 372, 155-163.

Rampoldi, L., F. Scolari, A. Amoroso, G. Ghiggeri, and O. Devuyst, 2011 The rediscovery of uromodulin (Tamm-Horsfall protein): from tubulointerstitial nephropathy to chronic kidney disease. Kidney Int, 80, 338-347.

Razzaque, M. S., 2011 Osteo-renal regulation of systemic phosphate metabolism. IUBMB Life, 63, 240-247.

Rowe, P. S., 2012 Regulation of bone-renal mineral and energy metabolism: the PHEX, FGF23, DMP1, MEPE ASARM pathway. Crit. Rev. Eukaryot. Gene Expr., 22, 61-86.

Rozman, J., M. Klingenspor, and M. Hrabě de Angelis, 2014 A review of standardized metabolic phenotyping of animal models. Mamm. Genome, 25, 497-507.

Sabrautzki, S., I. Rubio-Aliaga, W. Hans, H. Fuchs, B. Rathkolb *et al.*, 2012 New mouse models for metabolic bone diseases generated by genome-wide ENU mutagenesis. Mamm. Genome, 23, 416-430.

Saeed, A. I., N. K. Bhagabati, J. C. Braisted, W. Liang, V. Sharov *et al.*, 2006 TM4 microarray software suite. Methods Enzymol., 411, 134-193.

Saijoh, Y., H. Adachi, R. Sakuma, C. Y. Yeo, K. Yashiro *et al.*, 2000 Left-right asymmetric expression of lefty2 and nodal is induced by a signaling pathway that includes the transcription factor FAST2. Mol. Cell., 5, 35-47.

Schrimpf, C., C. Xin, G. Campanholle, S. E. Gill, W. Stallcup *et al.*, 2012 Pericyte TIMP3 and ADAMTS1 modulate vascular stability after kidney injury. J. Am. Soc. Nephrol., 23, 868-883.

Snoeckx, R. L., H. Kremer, R. J. Ensink, K. Flothmann, A. de Brouwer *et al.*, 2004 A novel locus for autosomal dominant non-syndromic hearing loss, DFNA31m maps to chromosome 6p21.3. J. Med. Genet., 41, 11-13.

Tan, A. and S. H. Ralston, 2014 Clinical presentation of Paget's disease: evaluation of a contemporary cohort and systematic review. Calcif. Tissue. Int., 95, 385-392.

Tanabe, M., A. Shimizu, Y. Masuda, M. Kataoka, A. Ishikawa *et al.*, 2012 Development of lymphatic vasculature and morphological characterization in rat kidney. Clin. Exp. Nephrol., 16, 833-842.

Tilyard, M. W., R. J. Gardner, L. Milligan, T. A. Cleary, and R. D. Stewart, 1982 A probable linkage between familial Paget's disease and the HLA loci. Aust. NZ. J. Med., 12, 498-500.

Tu, C. F., K. C. Tsao, S. J. Lee, and R. B. Yang, 2014 SCUBE3 (signal peptide-CUB-EGF domain-containing protein 3) modulates fibroblast growth factor signaling during fast muscle development. J. Biol. Chem., 289, 18928-42.

Tusher, V. G., R. Tibshirani, and G. Chu, 2001 Significance analysis of microarrays applied to the ionizing radiation response. Proc. Natl. Acad. Sci. U S A, 98, 5116-5121.

Van der Hauwaert, C., G. Savary, V. Gnemmi, F. Glowacki, N. Pottier *et al.*, 2013 Isolation and characterization of a primary proximal tubular epithelial cell model from human kidney by CD10/CD13 double labeling. PLoS One, 8, e66750.

Walker, K. A., S. Sims-Lucas, G. Caruana, L. Cullen-McEwen, J. Li *et al.*, 2011 Betaglycan is required for the establishment of nephron endowment in the mouse. PLoS One, 6, e18723.

Wang, L., L. Zhang, H. Yan, X. Liu, N. Li *et al.*, 2014 Genome-wide association studies identify the loci of 5 exterior traits in a Large White x Minzhu pig population. PLoS One, 9, e193766.

Whiteman, P., A. C. Willis, A. Warner, J. Brown, C. Redfield *et al.*, 2007 Cellular and molecular studies of Marfan syndrome mutation identify co-operative protein folding in the cbEGF12-13 region of fibrillin-1. Hum. Mol. Genet., 16, 907-918.

Wu, B. T., Y. H. Su, M. T. Tsai, S. M. Wasserman, J. N. Topper *et al.*, 2004 A novel secreted, cell-surface glycoprotein containing multiple epidermal growth factor-like repeats and one CUB domain is highly expressed in primary osteoblasts and bones. J. Biol. Chem., 279, 37485-37490.

Wu, Y. Y., K. Peck, Y. L. Chang, S. H. Pan, Y. F. Cheng YF *et al.*, 2011 SCUBE3 is an endogenous TGF-β receptor ligand and regulates the epithelial-mesenchymal transition in lung cancer. Oncogene, 30, 3682-3693.

Xavier, G. M., A. Economou, A. L. Senna Guimarães, P. T. Sharpe, and M. T. Cobourne, 2010 Characterization of a mouse Scube3 reporter line. Genesis, 48, 684-692.

Xavier, G. M., L. Panousopoulos, and M. Cobourne, 2013 Scube3 is expressed in multiple tissues during development but is dispensable for embryonic survival in the mouse. PLoS One, 8, e55274

Xu, Z. Y., S. M. Ding, L. Zhou, H. Y. Xie, K. J. Chen, W. Zhang *et al.*, 2012 FOXC1 contributes to microvascular invasion in primary hepatocellular carcinoma via regulating epithelial-mesenchymal transition. Int. J. Biol. Sci., 8, 1130-1141.

Yang, T., Y. G. Huang, I. Singh, J. Schnermann, and J. P. Briggs, 1996 Localization of bumetanide- and thiazide-sensitive Na-K-Cl cotransporters along the rat nephron. Am. J. Physiol., 271, F931-F939

Yang, R. B., C. K. Ng, S. M. Wasserman, S. D. Colman, S. Shenoy *et al.*, 2002 Identification of a novel family of cell-surface proteins expressed in human vascular endothelium. J. Biol. Chem., 277, 46364-46373.

Yang, H. Y., C. F. Cheng, B. Djoko, W. S. Lian, C. F. Tu *et al.*, 2007 Transgenic overexpression of the secreted, extracellular EGF-CUB domain-containing protein SCUBE3 induces cardiac hypertrophy in mice. Cardiovasc. Res., 75, 139-147.

Yang, M., M. Guo, Y. Hu, and Y. Jiang, 2013 Scube regulates synovial angiogenesis-related signaling. Med Hypotheses. 2013 Nov;81(5):948-53

Zhao, J., M Li, J. P. Bradfield, H. Zhang, F. D. Mentch *et al.*, 2010 The role of height-associated loci identified in genome wide association studies in the determination of pedriatric stature. BMC Med. Genet., 11: 96.

Zhao, C., Q. Gin, Q. Wang, J. Zhang, Y. Xu *et al.*, 2013 SCUBE3 overexpression predicts poor prognosis in non-small cell lung cancer. Biosci. Trends, 7&6, 264-269.

Zhou, D., R. J. Tan, L. Lin, L. Zhou, and Y. Liu, 2013 Activation of hepatocyte growth factor receptor, c-met, in renal tubules is required for renoprotection after acute kidney injury. Kidney Int., 84, 509-520.

FIGURES

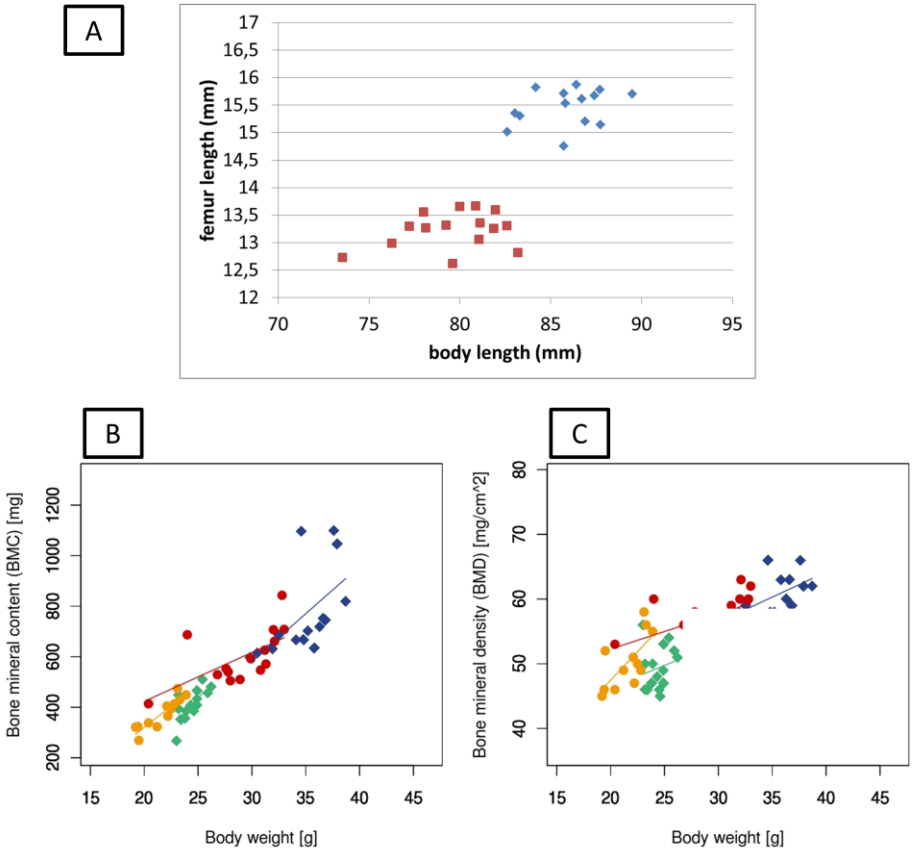

Figure 1

Skeletal abnormalities in *Scube3*$^{N294K/N294K}$ mice

A: femur length of female animals plotted by body length (red: *Scube3*$^{N294K/N294K}$, blue: *Scube3*^{WT}

B: Bone mineral content plotted by body weight (green: *Scube3*$^{N294K/N294K}$ males, yellow: *Scube3*$^{N294K/N294K}$ females, blue: *Scube3*^{WT} males, red: *Scube3*^{WT} females)

C: Bone mineral content plotted by body weight (green: *Scube3*$^{N294K/N294K}$ males, yellow: *Scube3*$^{N294K/N294K}$ females, blue: *Scube3*^{WT} males, red: *Scube3*^{WT} females).

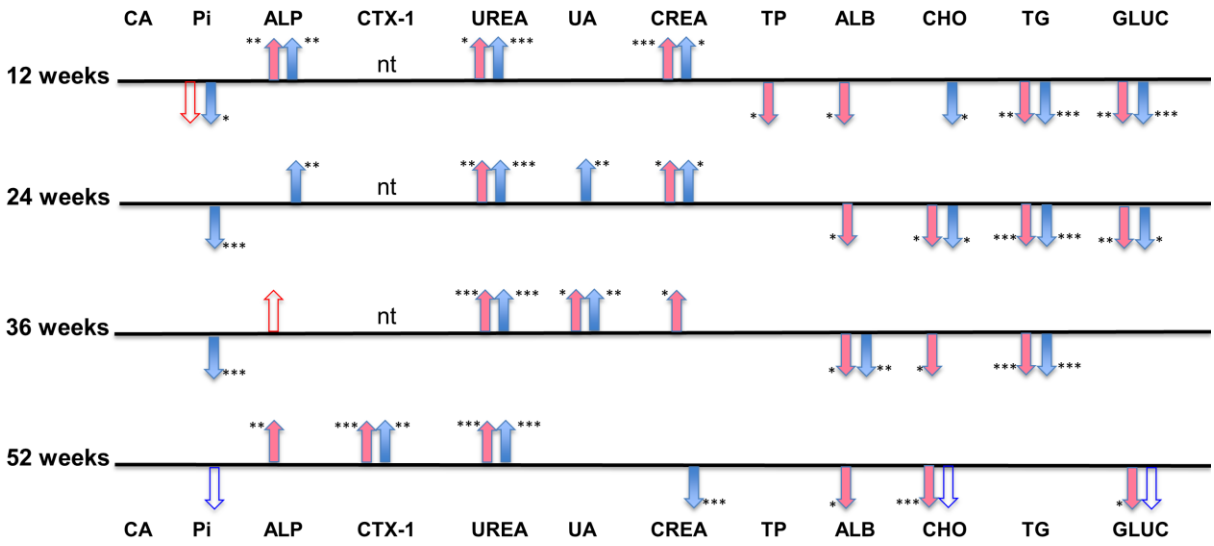

Figure 2

Statistically significant changed clinical chemical and CTX-1 plasma values of aged groups of *Scube3*$^{N294K/N294K}$ mice measured with 12, 24, 36 and 52 weeks of age.

Red resp. blue filled arrows show significantly increased or decreased plasma values for female and male mice compared to Scube3^{WT} mice (* = P≤0.05, ** ≤ P=0.01, ***P≤0.001; nt = not tested). Blanc but red resp. blue lined arrows show a tendency to increased or decreased values not reaching statistically significance.

Numbers of mice with 12 weeks were female *Scube3*$^{N294K/N294K}$ mice n = 9, female *Scube3*^{WT} n = 20, male *Scube3*$^{N294K/N294K}$ mice n = 21, male *Scube3*^{WT} n = 34; with 24 weeks female *Scube3*$^{N294K/N294K}$ mice n = 10, female *Scube3*^{WT} n = 21, male *Scube3*$^{N294K/N294K}$ mice n = 15, male *Scube3*^{WT} n = 29; with 36 weeks female *Scube3*$^{N294K/N294K}$ mice n = 12, female *Scube3*^{WT} n = 8, male *Scube3*$^{N294K/N294K}$ mice

n = 25, male *Scube3*^{WT} n = 33; with 52 weeks: female *Scube3*$^{N294K/N294K}$ mice n = 12, female *Scube3*^{WT} n = 8, male *Scube3*$^{N294K/N294K}$ mice n = 5, male *Scube3*^{WT} n = 11. For CTX-1 measurement with 52 weeks numbers were n = 10 mice for both female *Scube3*$^{N294K/N294K}$ mice and *Scube3*^{WT} mice, male *Scube3*$^{N294K/N294K}$ mice n = 9, male *Scube3*^{WT} mice n = 10.

Ca = total inorganic calcium; P_i = total inorganic phosphate; ALP = total alkaline phosphatase; CTX-1 = carboxy-terminal collagen crosslinks; UA = uric acid; CREA = creatinin; TP = total protein; ALB = albumin; CHO = cholesterol; TG = triglycerides; GLUC = glucose.

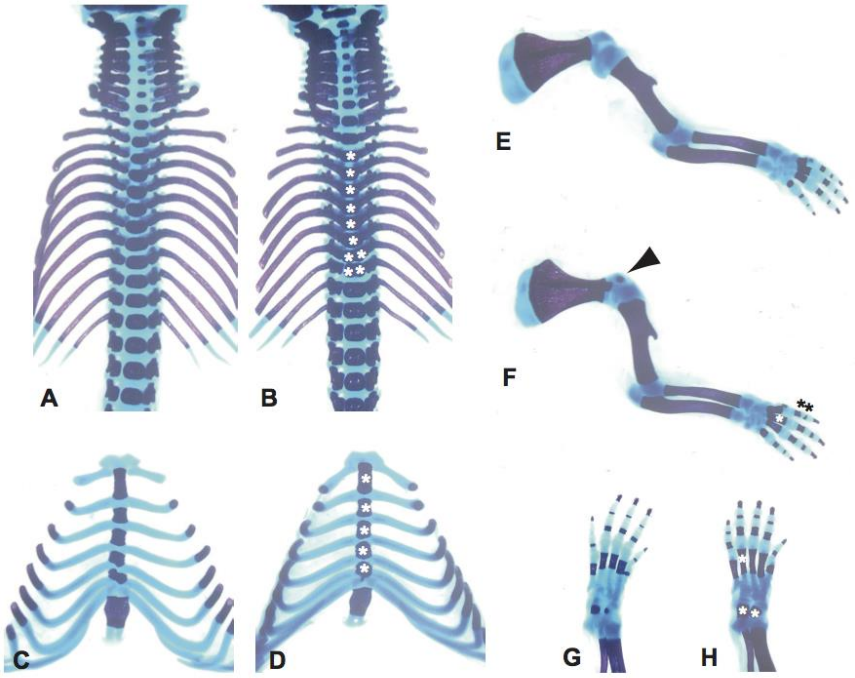

Figure 3

Skeletal phenotypes of newborn *Scube3*$^{N294K/N294K}$ mice.

Hyper-ossification of entire vertebrae in homozygous *Scube3*$^{N294K/N294K}$ mice (B, D) compared to wild type mice (A, C). Asterisks in (B) indicate remarkable hyper ossified vertebrae. Note that split ossification centers were detected in T10 and T11 (two asterisks in one vertebra). Sternebrae of *Scube3*$^{N294K/N294K}$ mice (C) were slightly thicker and longer than ones of wild type mice (D). Asterisks in (D) indicate hyper ossified sternebrae. Bones of upper and lower limbs in homozygous mutants (F, H) were also hyper-ossified compared to wild type (E, G). Arrowheads indicate ossified coracoid process (E) and tibia (H), respectively. Asterisks in (F) and (H) show representative hyper-ossified metacarpals, metatarsals, phalanx, and tarsals.

A

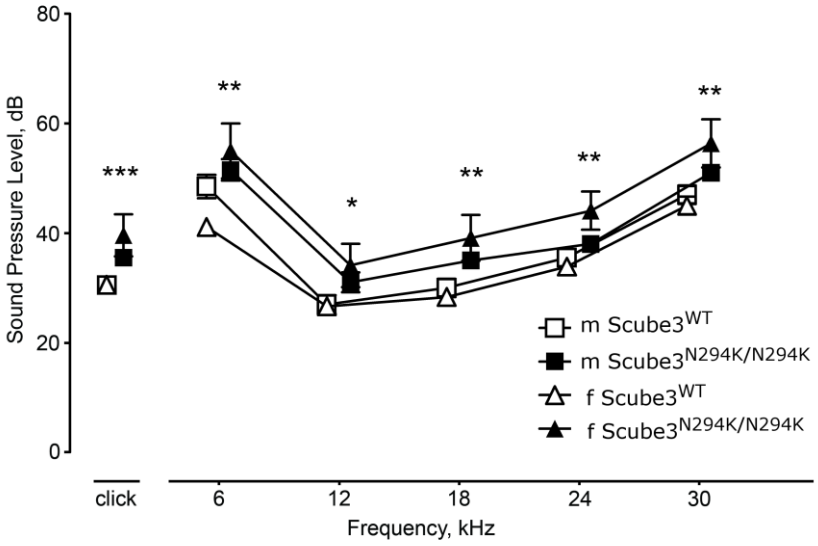

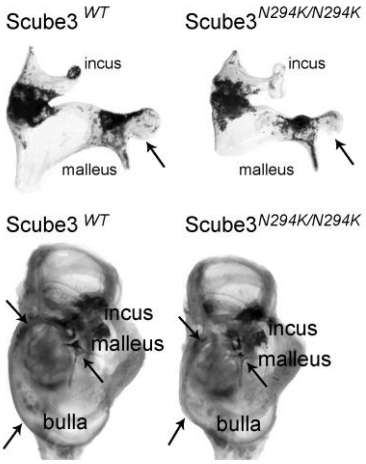

B

Figure 4

A: Mild conductive hearing loss; asterisks mark genotype effect of both sexes together * p<0.05, **p<0.01, *** p<0.001.

B: Abnormalities in inner ear development

Upper panel: depiction of smaller and malformed ossicles: the ambos (incus) has a different shape and especially the body of the hammer (malleus) is narrowed (arrow) and the head surface decreased.

Lower panel: the whole inner and middle ear was reduced in size and besides the alterations of the ossicles (arrow pointing towards the hammer, malleus), also the auditory cavity (bulla) has an irregular shape (arrows).

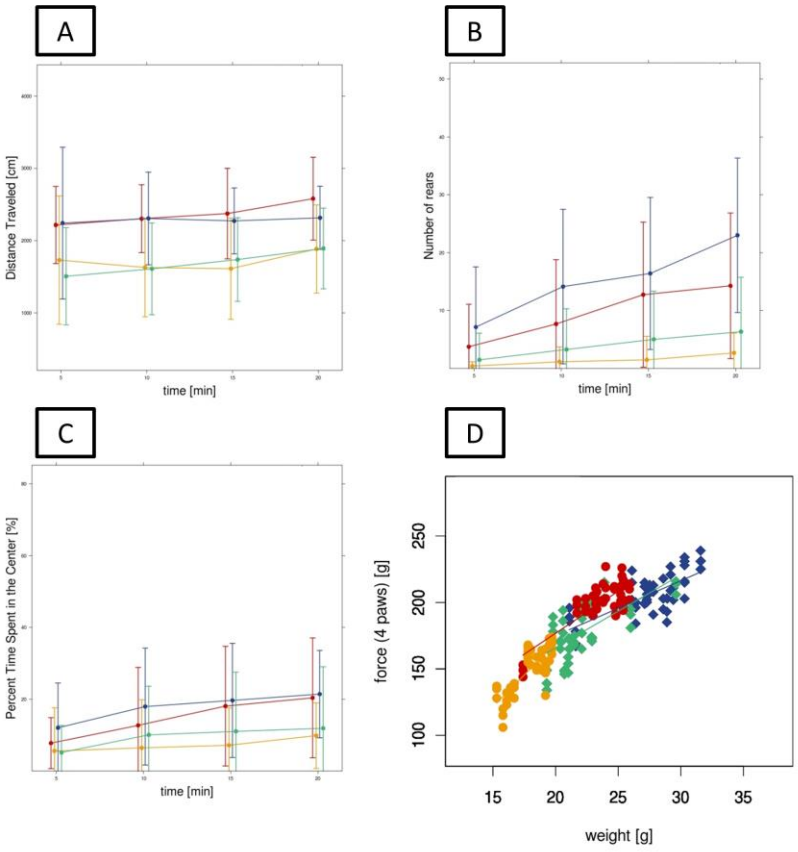

Figure 5

Analysis of *Scube3*$^{N294K/N294K}$ mice in the Open Field test and grip strength analysis. Data for distance travelled (A), number of rears (B) and percent time spent in centre (C) are shown over the 20 minutes test interval. Grip strength (4 paw measurement) is plotted versus body weight (D) (green: *Scube3*$^{N294K/N294K}$ males, yellow: *Scube3*$^{N294K/N294K}$ females, blue: *Scube3*^{WT} males, red: *Scube3*^{WT} females).

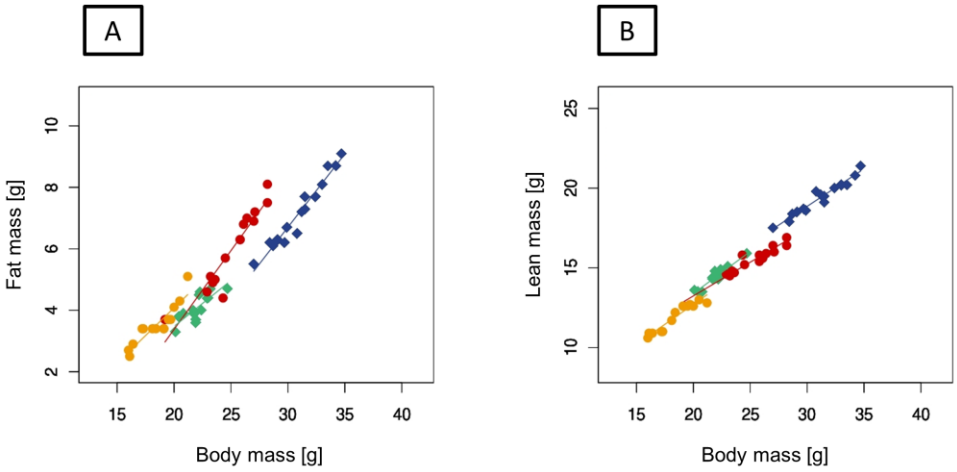

Figure 6

A: Fat mass plotted against body mass (green: *Scube3*$^{N294K/N294K}$ males, yellow: *Scube3*$^{N294K/N294K}$ females, blue: *Scube3*^{WT} males, red: *Scube3*^{WT} females)

B: Lean mass plotted against body mass (green: *Scube3*$^{N294K/N294K}$ males, yellow: *Scube3*$^{N294K/N294K}$ females, blue: *Scube3*^{WT} males, red: *Scube3*^{WT} females)

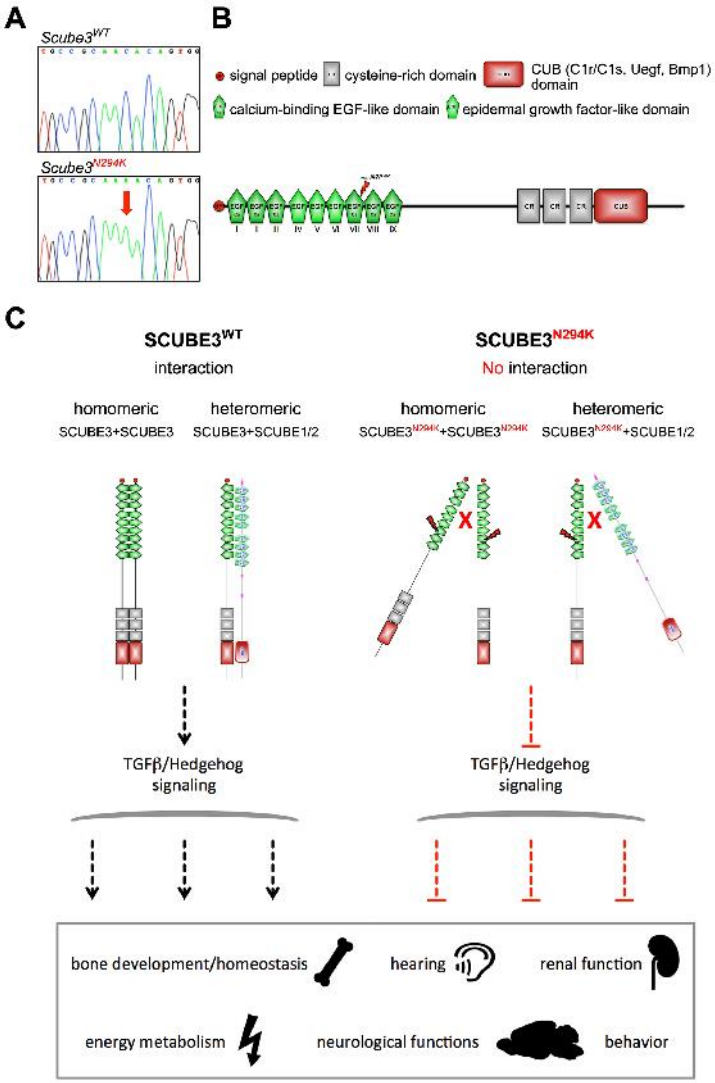

Figure 7

Scube3$^{N294K/N294K}$ mice are homozygous for a C to A point mutation at nucleotide position 882 that leads to an asparagine to lysine exchange at protein position 294 (N294K) in exon 8 of *Scube3 (A).* The mutation affects the calcium-binding EGF-like domain VII (B), which might have effects on the capabilities to form homo- or heterodimers and block TGFß/Hedgehog signaling (C), which causes phenotypic alterations in bone development and homeostasis, hearing ability, renal function, energy metabolism, neurological functions and behavior.

TABLES

Table 1: Renal function analysis

Sex		Males		females		2-way ANOVA	
Genotype	*Scube3*^{WT}	*Scube3*$^{N294K/N294K}$	*Scube3*^{WT}	*Scube3*$^{N294K/N294K}$	genotype	sex	genotype x sex
	n=12	n=12	n=10	n=12	p-value	p-value	p-value
Water uptake /25g BW [g/24h]	3.68 ± 0.81	6.01 ± 1.54	4.65 ± 1.88	6.88 ± 1.53	<0.001	0.039	0.910
Urine excretion/25g BW [g/24h]	0.59 ± 0.31	1.1 ± 0.43	0.89 ± 0.57	1.20 ± 0.55	0.004	0.201	0.412
Creatinine clearance/25g BW [µg/24h]	583 ± 305	548 ± 265	812 ± 564	606 ± 191	0.246	0.168	0.409
Na/25g BW [µmol/24h]	102 ± 50	208 ± 59	181 ± 105	205 ± 102	<0.001	0.004	0.803
K/25g BW [µmol/24h]	228 ± 109	444 ± 131	392 ± 237	539 ± 192	<0.001	0.014	0.510
Cl/25g BW [µmol/24h]	125 ± 62	262 ± 71	245 ± 154	364 ± 116	<0.001	<0.001	0.758
Ca/25g BW [µmol/24h]	1.2 ± 0.6	2.3 ± 0.8	2.7 ± 1.5	4.1 ± 1.4	<0.001	<0.001	0.611
Urea/25g BW [mg/24h]	60 ± 28.6	112 ± 31.9	111 ± 65.3	155 ± 44	0.099	<0.001	0.671
Total Protein/25g BW [mg/24h]	8.2 ± 3.5	11.8 ± 3.3	2.8 ± 1.9	3.7 ± 1.9	0.009	<0.001	0.107

Albumin/25g BW [µg/24h]	98 ± 39	122 ± 31	108 ± 44	153 ± 50	0.008	0.109	0.411
Glucose/25g BW [µg/24h]	210 ± 90	310 ± 94	427 ± 204	501 ± 121	0.030	<0.001	0.742
FE Na [%]	0.13 ± 0.05	0.30 ± 0.10	0.18 ± 0.05	0.33 ± 0.08	<0.001	0.149	0.656
FE K [%]	9.7 ± 3.1	20.4 ± 6.2	13.2 ± 3.3	21.7 ± 4.8	<0.001	0.082	0.422
FE Cl [%]	0.22 ± 0.08	0.52 ± 0.17	0.31 ± 0.08	0.57 ± 0.13	<0.001	0.061	0.672
FE Ca [%]	0.10 ± 0.03	0.20 ± 0.07	0.15 ± 0.02	0.28 ± 0.08	<0.001	<0.001	0.343
FE Urea [%]	19 ± 4.9	34 ± 10.4	28 ± 6.6	41 ± 10.5	<0.001	0.002	0.708
FE Total Protein [%]	0.007 ± 0.003	0.012 ± 0.006	0.027 ± 0.009	0.045 ± 0.012	<0.001	<0.001	0.016
FE Albumin [%]	0.00006 ± 0	0.00009 ± 0	0.00007 ± 0	0.00010 ± 0	<0.001	0.334	0.596
FE Glucose [%]	0.029 ± 0.009	0.043 ± 0.010	0.019 ± 0.007	0.031 ± 0.010	<0.001	<0.001	0.720

Table 2: Functional classification of regulated genes in kidney. Shown are significantly ($p<0.05$) enriched terms from the 'biological functions and disease' analysis in Ingenuity Pathway Analysis

Biological functions & disease	**Genes**	**# genes**
cellular development	*Blk, Casp3, Ccr1, Chek1, Commd3-Bmi1, Cxcl12, Eif4g2, Ereg, Foxc1, Gabpa, Has2, Havcr1, Hif1a, Hmox1, Hoxa10, Id4, Igf2, Jdp2, Met, Rasgrp1, Scel, Srpx2, Tcf21, Tert, Tnn*	25
cellular movement	*Adamts1, Arhgap35, Ccr1, Cxcl12, Ereg, Foxc1, Fpr3, Has2, Hif1a, Hmox1, Igf2, Ltc4s, Mep1b, Met, Mme, Plec, Ppt2, Rasgrp1, Sema6d, Slc12a1, Srpx2, Tgfbr3, Tnn, Umod, Vav3*	25
cardiovascular system function	*A4gnt, Adamts1, Casp3, Chm, Cxcl12, Ehd3, Foxc1, Has2, Hif1a, Hmox1, Hoxa10, Ift57, Igf2, Lefty2, Met, Plec, Srpx2, Tcf21, Tert, Tgfbr3, Tnn, Trpc1, Usp8, Vav3*	24
nervous system function	*Arhgap35, Casp3, Chm, Commd3-Bmi1, Cxcl12, Fa2h, Faim2, Gpr37, Hif1a, Hoxa10, Ift57, Igf2, Madd, Met, Plec, Ppt2, Rgs7, Sh3gl2, Slitrk6, Vav3*	20
cell death and survival	*Adamts1, C8orf44-Sgk3/Sgk3, Casp3, Ccr1, Chek1, Commd3-Bmi1, Cxcl12, Fa2h, Hif1a, Hmox1, Id4, Igf2, Jdp2, Met, Tert, Top1, Umod, Usp8*	18
neurological disease	*Casp3, Commd3-Bmi1, Gnat1, Gng7, Grik1, Hmox1, Id4, Igf2, Kcnip2, Man1a1, Mdh1, Ppp1cb, Ppt2, Ranbp1, Sgtb, Sh3gl2, Top1*	17
cancer	*Acta2, Bdh1, Gpr37, Havcr1, Hif1a, Hmox1, Id4, Igf2, Lefty2, Mdh1, Met, Tert, Tgfbr3*	13
cell cycle	*Chek1, Commd3-Bmi1, Has2, Havcr1, Hmox1, Hoxa10, Id4, Igf2, Met, Slbp, Tert, Trpc1, Usp8*	13
cellular growth and proliferation	*Chek1, Cxcl12, Ereg, Ghrhr, Has2, Hif1a, Hoxa10, Id4, Lmo3, Met, Tert, Top1*	12
developmental disorder	*Chm, Commd3-Bmi1, Eif4g2, Has2, Hif1a, Hmox1, Ift57, Igf2, Ranbp1, Sh3gl2, Slc12a1, Usp8*	12
renal and urological disease	*Ccr1, Ereg, Havcr1, Hif1a, Igf2, Lmo3, Met, Mme, Slc39a8, Tert*	10